The Influence of Forests on Atmospheric Heating during the Snowmelt Season

TAKESHI YAMAZAKI

Geophysical Institute, Tohoku University, Sendai, Japan

(Manuscript received 9 November 1993, in final form 29 June 1994)

ABSTRACT

Atmospheric heating during the snowmelt season has been studied by means of data analysis and numerical model experiments. As a result of the data analysis, it was shown that in some examples the daytime air temperature rose above 0°C, even if the ground surface was covered by snow. Moreover, it was found that the number of days when the daytime air temperature rose above 0°C was large when the duration of sunshine increased. However, the increase was not related to the wind speed. Therefore, the air temperature over snow cover increases during the daytime if the sunshine is strong even under calm conditions (weak advection). On the other hand, the following result was obtained with the use of a local circulation model combined with a canopy heat balance model. The atmosphere was heated over the plains if forested areas existed around the plains, even if the plains surfaces were covered by snow without forests. An upward sensible heat flux was supplied from the forest canopy, resulting in atmospheric heating. It was concluded that the existence of forests was one of the main causes of atmospheric heating during the snowmelt season.

1. Introduction

It has often been experienced that the daytime surface air temperature rises above 0°C, even if the ground is covered by snow. This is contrary to intuition since the temperature of snow never rises above 0°C. Possible causes of atmospheric heating during the snowmelt season are advection, heat from obstacles, direct heating by solar radiation, mesoscale subsidence due to the terrain (similar to a foehn wind), and synoptic-scale subsidence. The state of the lower atmosphere depends on these conditions, especially the first two. In this paper, we take note mainly of the influence of obstacles such as forest.

Yamazaki and Kondo (1992) discussed the heat balance and snowmelt in snow-covered forested areas using a heat balance model of the forest coupled with a snowmelt model. Moreover, Yamazaki and Kondo (1993) showed using a one-dimensional numerical model that an upward sensible heat flux from the forest canopy caused the air temperature to rise above 0°C. The conditions for the calculation are a geostrophic wind velocity of 5 m s^{-1} and a snow albedo of 0.6. The initial potential temperature (at midnight) is given with the gradient $\Gamma = 0.004$°C m^{-1} and an initial relative humidity at the surface of 50%. Figure 1 shows the relationship between the canopy density c_* [see Yamazaki et al. (1992) as the definition] and the maximum value of the sensible heat flux H_{max} from the ground surface to the atmosphere and the daily maximum temperature T_{max} (at $z = 10$ m). Two calculations are shown: one for an initial potential temperature T_{Si} of 0°C at the surface (thick lines) and one for −5°C (thin lines). The value of H_{max} reaches 100 W m^{-2} for a sparse canopy ($c_* \approx 0.1$: leafless deciduous forest), while the value of T_{max} becomes greater than 0°C if $T_{Si} > -5$°C. The value of T_{max} changes, it can be seen, due to the initial temperature profile. However, the sharp increase in T_{max} to temperatures higher than 0°C does not occur without the influence of forests ($c_* \approx 0.001$). If the forest is dense ($c_* > 1$: tall coniferous forest), the value of H_{max} becomes greater than 300 W m^{-2}, and the depth of mixed layer reaches 1700 m determined with the calculated potential temperatures and diffusivities. It is found that when a forest exists the atmosphere can be heated, even if the ground is covered by snow. The above results indicate that forests probably influence the climate during the snowmelt season.

However, since portions of the plain area may be cultivated, they often become a flat snow surface during the winter. Usually, only the hilly districts around the plain are mostly forested. In this case, it is expected that the local circulation will influence the atmospheric heating.

While upslope flows are present even during the snow season in an evergreen-covered valley, the actual mechanism for such winds is not yet clearly understood (Whiteman 1990). Such an upslope flow is the evidence that sensible heat is supplied to the atmosphere. Segal et al. (1991) simulated the "snow breeze," which is a local circulation resulting from horizontal thermal

Corresponding author address: Takeshi Yamazaki, Geophysical Institute, Tohoku University, Aza-Aoba Aramaki, Aoba-ku, Sendai 980-77, Japan.

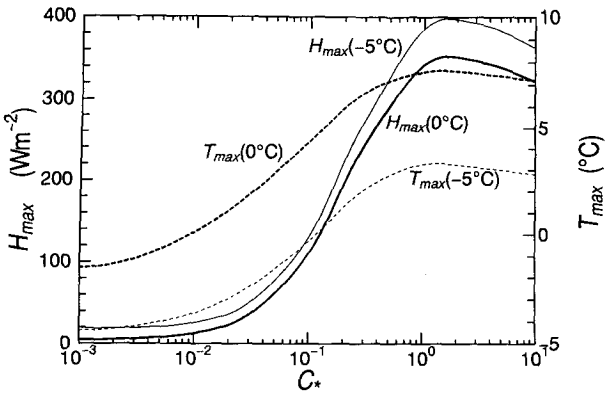

FIG. 1. Relationship between the canopy density c_*, the maximum sensible heat H_{max}, and the daily maximum temperature T_{max} (z = 10 m) for the first day of the calculation. The parameter in parentheses is the initial air temperature at the ground surface T_{Si}.

gradients between snow-covered and snow-free areas during the daytime. They also mentioned the sensible heat flux from a canopy surface with snow cover.

In the present paper, the mechanism of the air temperature increase over the plains during the snowmelt season will first be investigated by the data analysis. The effect of forests on the atmospheric heating will then be studied with the use of an atmospheric model combined with canopy and snowmelt models.

2. Description of the method

a. Data analysis

The Automated Meteorological Data Acquisition System (AMeDAS) was established by the Japan Meteorological Agency. The AMeDAS data analyzed here are taken from Niigata Prefecture, which has a wide plain in its center, being one of the highest areas of snowfall in Japan (Fig. 2). Although several cities are located on the plain, a large area is covered by paddy fields.

The relationship between some meteorological conditions and atmospheric heating will be investigated statistically. Ten stations at a distance of more than 10 km from the coast were selected from the AMeDAS stations in Niigata Prefecture. The sea may influence the air temperature near the sea. Thus, we omitted the stations at a distance of less than 10 km from the coast. The stations at Niitsu and Sanjo are also far from the coast, but these two stations were rejected because the snow is light there. The mechanism for the air temperature increase was examined for the days when the snow cover was deeper than 30 cm at Nagaoka, a station with the lightest snow, for February and March, from 1980 to 1992.

b. Model

It is difficult to separate the influence of obstacles (forest) by only data analysis. Therefore, it will be investigated with the use of a model.

1) THE ATMOSPHERIC MODEL

The details of the atmospheric model have been described in Kimura and Manins (1988). The Coriolis term and the equation for specific humidity are added. The basic equations are simplified by the Boussinesq and hydrostatic approximations, as

$$\frac{\partial h_a u}{\partial t} + \frac{\partial h_a uu}{\partial x} + \frac{\partial h_a uw^*}{\partial z^*} = fh_a v - h_a \Theta \frac{\partial \pi'}{\partial x} + gh_a \frac{\theta'}{\Theta} \frac{z_t - z^*}{z_t} \frac{\partial z_g}{\partial x} + \frac{\partial}{\partial x}\left(h_a K_H \frac{\partial u}{\partial x}\right) + \frac{z_t^2}{h_a} \frac{\partial}{\partial z^*}\left(K_m \frac{\partial u}{\partial z^*}\right), \quad (1)$$

$$\frac{\partial h_a v}{\partial t} + \frac{\partial h_a vu}{\partial x} + \frac{\partial h_a vw^*}{\partial z^*} = -fh_a u + \frac{\partial}{\partial x}\left(h_a K_H \frac{\partial v}{\partial x}\right) + \frac{z_t^2}{h_a} \frac{\partial}{\partial z^*}\left(K_m \frac{\partial v}{\partial z^*}\right), \quad (2)$$

$$\frac{\partial h_a \theta'}{\partial t} + \frac{\partial h_a \theta' u}{\partial x} + \frac{\partial h_a \theta' w^*}{\partial z^*} = \frac{\partial}{\partial x}\left(h_a K_H \frac{\partial \theta'}{\partial x}\right) + \frac{z_t^2}{h_a} \frac{\partial}{\partial z^*}\left(K_h \frac{\partial \theta'}{\partial z^*}\right), \quad (3)$$

$$\frac{\partial h_a u}{\partial x} + \frac{\partial h_a w^*}{\partial z^*} = 0, \quad (4)$$

$$\frac{\partial \pi'}{\partial z^*} = \frac{h_a}{z_t} \frac{g\theta'}{\Theta^2}, \quad (5)$$

and

$$\frac{\partial h_a q}{\partial t} + \frac{\partial h_a uq}{\partial x} + \frac{\partial h_a qw^*}{\partial z^*} = \frac{\partial}{\partial x}\left(h_a K_H \frac{\partial q}{\partial x}\right) + \frac{z_t^2}{h_a} \frac{\partial}{\partial z^*}\left(K_h \frac{\partial q}{\partial z^*}\right). \quad (6)$$

Here u, v, and w^* are the wind velocities; θ' is the deviation of potential temperature from the mean potential temperature Θ; q the specific humidity; and f the Coriolis parameter. The terrain-following vertical coordinate z^* is defined by

$$z^* = z_t \frac{z - z_g}{h_a}, \quad h_a = z_t - z_g,$$

in which z_t and z_g are the respective levels of the top and ground surfaces of the model atmosphere, K_H is the horizontal diffusivity, and K_m and K_h the vertical diffusivity for momentum and heat, respectively. The minimum values of K_m and K_h are set at 0.5 m^2 s^{-1} to avoid the appearance of extremely small values under

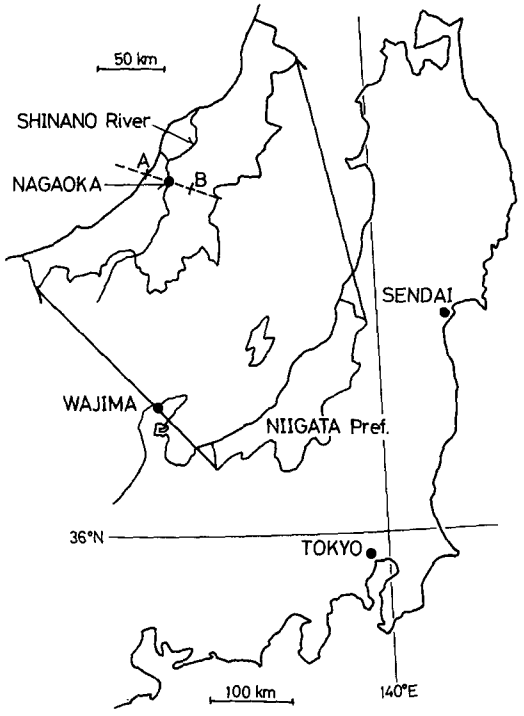

FIG. 2. A map of eastern Japan showing the location of Niigata Prefecture.

strong stable conditions. Longwave radiative cooling of the atmosphere is accounted for by the parameterization discussed in Kondo and Matsushima (1993).

2) THE CANOPY MODEL (TWO-LAYER MODEL)

The details of this model and its performance have been described in a previous paper (Yamazaki et al. 1992). The fluxes above and in the canopy can be calculated with the use of this model, if incident solar and infrared radiation, air temperature, specific humidity, and wind speed are given as input parameters. The canopy is divided into a "crown space" and "trunk space" (without leaves), with the crown space subdivided into two layers. The heat balance is solved with respect to the radiative, sensible, and latent heat fluxes among the atmosphere and the two crown layers.

The sensible and latent heat fluxes can be described as proportional to the differences of temperature and specific humidity, respectively. The effect of atmospheric stability between the top of the canopy and the lowest layer of the atmospheric model is taken into account with the use of shear functions obtained from the data of Kondo et al. (1978) and Dyer and Hicks (1970).

3) THE SNOWMELT MODEL

The details of the snowmelt model were described in Kondo and Yamazaki (1990). This model simultaneously calculates the snow-surface temperature and freezing depth, taking into consideration the nocturnal refreezing of the liquid water in the snow cover. Part of the incident solar radiation is transmitted into the interior of the snow cover, which is also considered. The sensible and latent heat fluxes are parameterized by bulk formulas and a linear temperature profile is assumed in the snow cover. Thus, the heat balance equations for both the snow surface itself and for the entire snow cover can be solved.

4) ASSUMPTIONS OF THE TWO-DIMENSIONAL CALCULATION

Figure 3a displays the cross section of elevation along the broken line AB in Fig. 2. The plain surrounded by forested hills is widely used as paddy fields and becomes a snowfield in the winter. The Shinano River flows across the center of the plain, from south to north, and the terrain can be considered as two-dimensional. Therefore, the terrain and surface conditions displayed schematically in Fig. 3b are selected for the calculations.

It is assumed that the plain is covered by snow only and that the surrounding hilly region is covered by forest [medial dense: $c_* = 0.3$, evapotranspiration factor of a leaf $j = 0.1$; see Yamazaki et al. (1992) as the definition] with snow covering the ground under the forest canopy. The width of the calculated area $2W$ is set to 20 km, and the height of the hill h_0 as 300 m. The model atmosphere is divided into 29 layers in the vertical with a grid interval of 5 m at the lowest and about 400 m at the top (the model top height is 4200 m), and a horizontal grid interval is 1 km. The upper boundary condition is the gravity wave radiation condition presented by Klemp and Durran (1983) and Bougeault (1983). The lateral boundary conditions are periodic. The initial potential temperature θ_i is linear in height, given as

$$\theta_i(z) = \Gamma z + T_{Si} \qquad (7)$$

at model time 0200 (started from rest). Conditions of the control run are as follows: the gradient of potential temperature $\Gamma = 0.005°\text{C m}^{-1}$, initial potential temperature at the surface $T_{Si} = 0°\text{C}$, and the geostrophic wind at the top of the model atmosphere is 0.

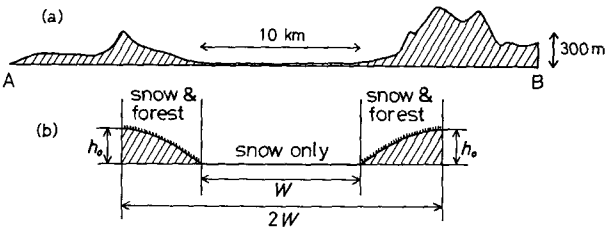

FIG. 3. (a) The cross section of elevation above sea level along the broken line AB in Fig. 2 and (b) the schematic illustration of the terrain and surface conditions in the numerical model.

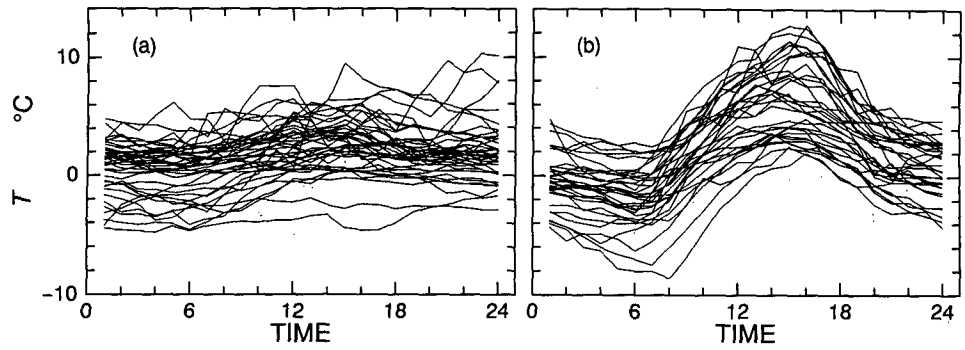

FIG. 4. Time series of air temperatures at Nagaoka. The range of wind speed during the temperature observation was from 1 to 2.5 m s^{-1}; for the duration of sunshine (a) $N = 0$ and (b) $N \geq 9$ h.

3. Results

a. Data analysis

Figure 4 shows the time series of air temperature at Nagaoka when the wind speed ranged from 1 to 2.5 m s^{-1}. Figure 4a shows the data for the sunshine duration of zero, and Fig. 4b when more than 9 h. The latitude of the test area is 38°N; the possible daily duration of sunshine (daytime length) is 10.3 h on 1 February, changing to 12.6 h on 31 March. This is a very cloudy region in winter climatologically; it is cloudier in February than March in this region.

Figure 4a shows little tendency for diurnal variation when the sunshine duration is zero. The diurnal variations are closely related to the solar radiation; however, advection takes part in warm temperature because there are many curves that show air temperatures above 0°C in Fig. 4a. Although figures are omitted, similar features are found at the other nine stations besides Nagaoka.

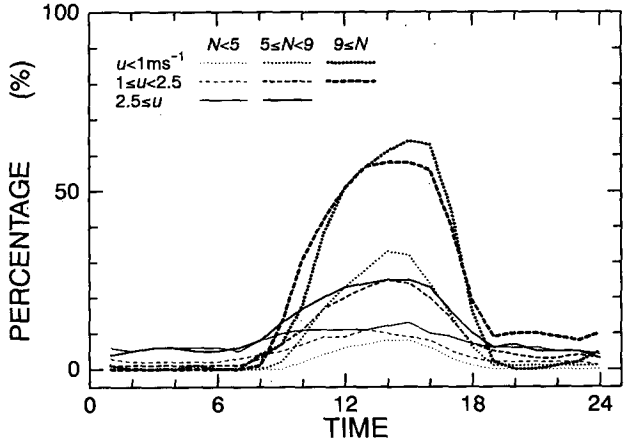

FIG. 5. The percentage of number of occurrences when the air temperature rises above 5°C from hourly surface observations. The thickness of each line denotes the duration of sunshine N: thin lines $N < 5$ h, middle lines 5 h $\leq N < 9$ h, and thick lines $N \geq 9$ h. The type of line indicates the wind speed u: dotted lines $u < 1$ m s^{-1}, broken lines 1 m $s^{-1} \leq u < 2.5$ m s^{-1}, and solid lines $u \geq 2.5$ m s^{-1}.

Figure 5 shows the percentage of number of occurrences when the air temperature rises above 5°C at the 10 stations. For the eight lines in this figure, the thickness of each line denotes the duration of sunshine N as thin lines $N < 5$ h, medium lines 5 h $\leq N < 9$ h, and thick lines $N \geq 9$ h. Moreover, the type of line indicates the wind speed u as dotted lines $u < 1$ m s^{-1}, broken lines 1 m $s^{-1} \leq u < 2.5$ m s^{-1}, and solid lines as $u \geq 2.5$ m s^{-1}. Table 1 lists the number of data in each category. The category for $N \geq 9$ h and $u \geq 2.5$ m s^{-1} has been removed from Fig. 5 as a result of too few data in this category.

In Fig. 5 the percentage of surface observations when the temperature exceeds 5°C is shown to depend almost exclusively on the duration of sunshine, being nearly independent of the wind speed. Therefore, it can be concluded that when the ground is snow covered, atmospheric heating is influenced by solar radiation rather than by advection. However, the snow albedo is high, which means the ground does not absorb solar radiation effectively, the snow temperature never rises above 0°C, and some heat goes into melting the snow. Thus, obstacles such as forests probably take part in causing the air temperature to rise above the melting point.

Examples of atmospheric heating during the snowmelt season were selected for February and March, from 1980 to 1991. First, about 30 calm days were selected based on synoptic weather chart. Next, criteria for the selection of the examples are based on the data at Nagaoka (in central Niigata) as follows: the snow

TABLE 1. The number of data in each category shown in Fig. 5.

	$N < 5$	$5 \leq N < 9$	$9 \leq N$
$u < 1$ m s^{-1}	929	376	131
$1 \leq u < 2.5$	1286	718	233
$2.5 \leq u$	582	128	33

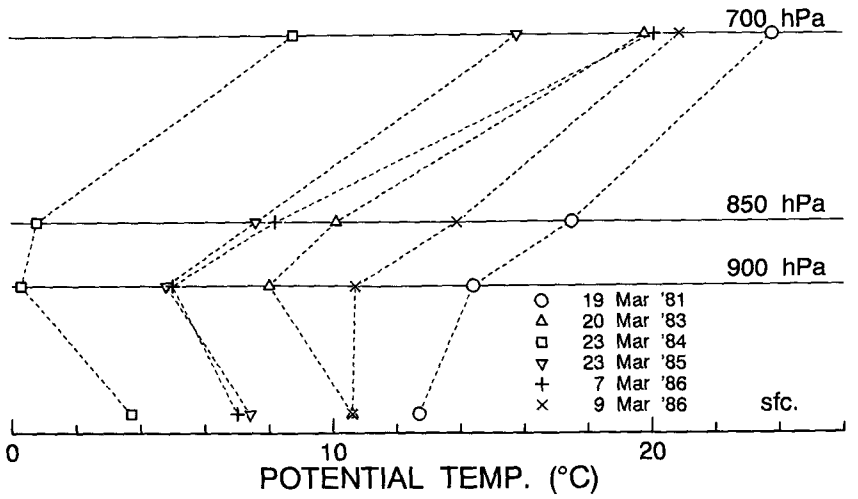

FIG. 6. Profiles of potential temperature and maximum air temperature at Nagaoka for the selected 6 days. The figure legend indicates the days.

depth was at least 30 cm, the daily mean wind speed was at most 2 m s^{-1} (slight or no advection), and the duration of sunshine was at least 10 h (the atmosphere was not heated when the insolation was weak). Six days were found to satisfy the three criteria mentioned above.

Figure 6 shows the profiles of potential temperature and the maximum surface air temperature at Nagaoka for the 6 days. Since we have no available aerological data in Niigata Prefecture, the data at Sendai (200 km east-northeast of Nagaoka; see Fig. 2) and Wajima (160 km west of Nagaoka) are employed. The upper-air potential temperatures (at the 900-, 850-, and 700-hPa levels) are the average of those at 2100 JST the day before the selected day and those at 0900 JST on the day at Sendai and Wajima. The vertical gradients of potential temperature Γ range from 0.004° to 0.005°C m^{-1}; these values have been used as initial conditions in the numerical experiments. The lower atmosphere seems to be unstable or neutral despite the snow cover, indicating the occurrence of vertical mixing. Although the actual distribution of the potential temperature between the surface and 900 hPa is unknown, the lower atmosphere may have a structure like a mixing layer. The upper winds at 0900 JST are shown in Table 2 for these days. Since there is not always a slight wind blowing at the level of 850 or 700 hPa, it is difficult to judge which process is actually dominating, heat from obstacles or advection, from aerological data.

Figure 7 displays the distribution of the surface air temperature and the wind vector at 0500 and 1400 JST for 9 March 1986 as a typical example. At 0500, the air temperature dropped below the freezing point except for some part. On the other hand, the 1400 JST air temperature increased to higher than 10°C along the coastal regions, and from 6° to 8°C over inland areas. The range of sea surface temperature from the Geostationary Meteorological Satellite (GMS) data was 8°–11°C (averaged from 1 to 10 March 1986). However, the surface wind vector distribution reveals that no clear wind system dominates, and the winds are basically calm.

b. Numerical experiment

Figure 8 illustrates the streamlines and potential temperature cross sections, respectively, at 0500 JST, while those at 1400 JST are shown by Fig. 9. At 0500, after 3 h of simulated time, very slight cold-air drainage from the hilly region to the plain is calculated; however, the field of potential temperature is almost the same as the initial field. At 1400, the wind from the plain (snow cover only) to the hilly region becomes notable, with a wind speed of 1–2 m s^{-1}. The return current is found between 700 and 1000 m. Moreover, a mixed layer extends to a height of more than 1000 m, although a shallow stable layer persists below 400 m over the plain. The lower atmosphere over the center of the

TABLE 2. The upper-wind direction (D: deg) and wind speed (U: m s^{-1}) at 0900 JST.

	Sendai				Wajima			
	850 hPa		700 hPa		850 hPa		700 hPa	
Date	D	U	D	U	D	U	D	U
19 March 1981	244	10	245	13	241	9	274	8
20 March 1983	255	9	287	15	248	8	246	11
23 March 1984	352	11	303	9	347	5	319	13
23 March 1985	324	7	279	13	51	3	256	8
7 March 1986	301	11	304	14	251	3	289	9
9 March 1986	276	16	265	17	248	13	252	17

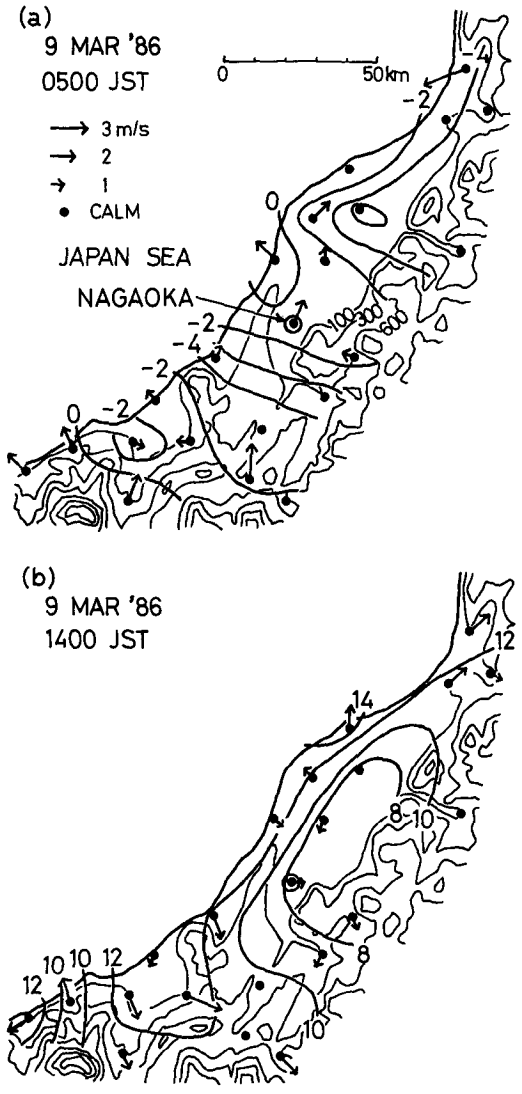

FIG. 7. Horizontal distribution of surface air temperature and wind vectors at (a) 0500 JST and (b) 1400 JST 9 March 1986. The thick curves denote isothermal lines. The length of the vector denotes the wind speed according to the legend.

plain is heated by subsidence; the maximum value of the downward vertical velocity is 0.15 m s^{-1} at the level of 600 m. The atmosphere above 1200 m cools due to longwave radiative cooling by 0.3°–0.5°C between 0500 and 1400 JST.

Figure 10 shows time series of the sensible heat flux and air temperatures at the height of 5 m on both the top of the hill and on the center of the plain. The thick lines denote the control run (no geostrophic wind, T_{Si} = 0°C, h_0 = 300 m). While the maximum sensible heat supplied to the atmosphere is about 250 W m^{-2} over the forested area (broken line), the sensible heat flux over the plain is almost zero (solid line). Therefore, the sole source of heat flux to the atmosphere is supplied from the forested area. The heating of the atmosphere over the plain through subsidence is similar to the heating in a valley and over a basin bottom during nonsnow seasons (Whiteman 1982; Kondo et al. 1989). However, during nonsnow seasons the sensible heat from the floor is large, besides the subsidence.

The dependence of sensible heat and air temperature on some parameters is also shown in Fig. 10. The sensible heat fluxes at hilltop do not have large differences, with a maximum value of 240–270 W m^{-2}. On the other hand, at the center of plain, the sensible heat fluxes are almost zero except for run U5.

On run U5 (geostrophic wind is 5 m s^{-1}), in which forced wind is blowing, the sensible heat flux of about 20 W m^{-2} is transferred to the snow surface. Thus, the lowest atmosphere is cooled at the plain center, especially in morning. The same situation is found at the hilltop before dawn, corresponding the downward sensible heat flux with a value of 40 W m^{-2}.

Figure 11 shows the streamlines and potential temperature when geostrophic wind is 5 m s^{-1}. A well-mixed layer occurs, having similar thickness with the control run, even if different geostrophic winds are given; however, wind circulation is collapsed. Although a stagnated area occurs under 300 m, it flows uniformly over 500 m. Since the stagnation region is easily disturbed by ambient flow, it may be difficult to observe this kind of circulation at the surface. The result when geostrophic wind is 10 m s^{-1} is similar, but the stagnated area becomes smaller.

The heating of the lower atmosphere over the plain is only weakly dependent on the height of the hill (Fig. 10, run H5 and H0). According to calculations with various hill heights, the circulation is only slightly stronger when the hill is low (including h_0 = 0). As the hill becomes lower, the thickness of the stable layer over the plain becomes shallower; it is the same as or slightly thinner than the height of the hill. However, the air temperature at the surface of the plain does not change. The hill height is not essential since the circulation and atmospheric heating depend on the horizontal variability of ground surface characteristics such as whether forests are present or not. Therefore, this circulation more resembles a sea–land breeze or a "snow breeze" than valley (or slope) wind. The air temperature at the hilltop depends on the hill height h_0, because the elevation where the air temperature is taken from the plain level varies with h_0.

When the initial potential temperature is raised by 5°C, the calculated surface air temperature increases by 4°–5°C (Fig. 10, run T5). Although the sensible heat flux supplied to the atmosphere over the hill is slightly smaller, the way of temperature rising is almost the same. A strong stable layer occurs just above the snow surface over the plain.

4. Discussion

In this section, a comparison is first made between the observed air temperature and the calculated results.

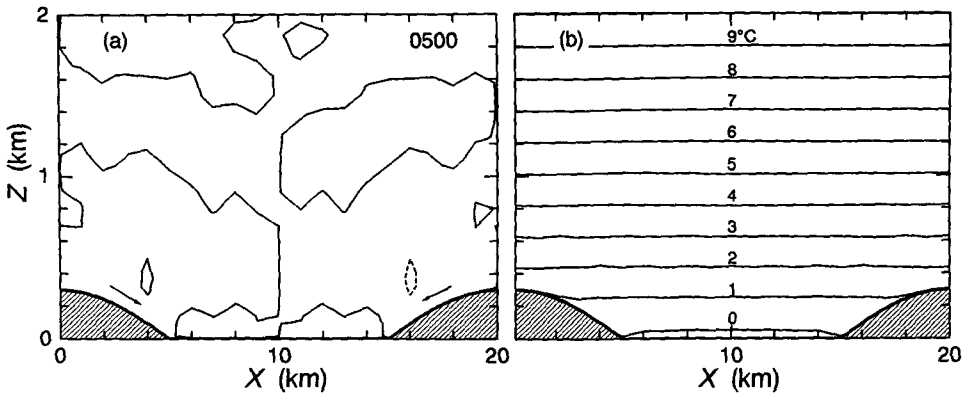

FIG. 8. (a) Calculated streamlines and (b) potential temperature at the model time 0500 JST. The broken streamline denotes negative values. The arrows in (a) indicate the direction of the wind. The contour interval of the streamlines is 20 $m^2 s^{-1}$.

For the selected day of 9 March 1986, as shown in Fig. 6, the actual potential temperature in the upper region (900–700 hPa) is close to the calculated value with $\Gamma = 0.005°C\ m^{-1}$ and $T_{Si} = 5°C$ (same as run T5 in Fig. 10). After comparing Fig. 7 with the calculation (run T5 in Fig. 10), the calculated air temperature of about 6°C at 1400 JST is similar to or slightly lower than the actual temperatures of 8°–10°C. The observed screen height temperature is below the freezing point at 0500 JST; however, the calculated temperature drops to only 4°C at the center.

Concerning this result, two problems are found. The first is that the initial time and the initial temperature profile near the ground are unsuitable. It could be that the atmosphere near the ground is cooled, and the mixed layer formed during the previous day remains. The other problem of air temperature discrepancy is the height at which the air temperature is taken. The height of the lowest grid point in the model is 5 m compared with the observed height of 1–2 m. In fact, the calculated snow surface temperature exhibits a significant drop, reaching a minimum of −8.1°C in run T5 in Fig. 10. The atmospheric model is not a model to predict the air temperature at the lowest layer exactly. Furthermore, since there is a problem of radiative absorption as mentioned in the introduction, it is not so significant to simulate the surface air temperature itself completely. That is, the atmosphere is so heated that the deep mixed layer occurs.

The actual surface screen air temperature is close to the calculated potential temperature in the mixed layer during the daytime. The height of the mixed layer extends to about 1000 m (900 hPa) in the calculated results. Figure 12 displays the relationship between the daily maximum surface air temperature at Nagaoka and the mean potential temperature at 900 hPa, which is the averaged temperature at 2100 JST from the preceding day and at 0900 JST of the day over the two stations, Sendai and Wajima. A linear relationship is found in this figure, and they have similar values when the temperatures are higher. Since it is unrealistic that the lower atmosphere is highly unstable, the maximum air temperature at the surface must be close to the potential temperature in the mixed layer. Therefore, if it

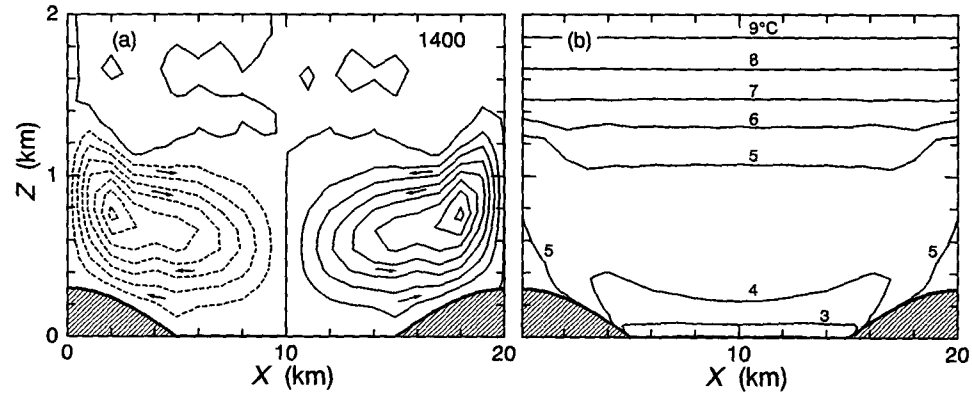

FIG. 9. The same as Fig. 8 except at 1400 JST. The contour interval of the streamlines is 100 $m^2 s^{-1}$.

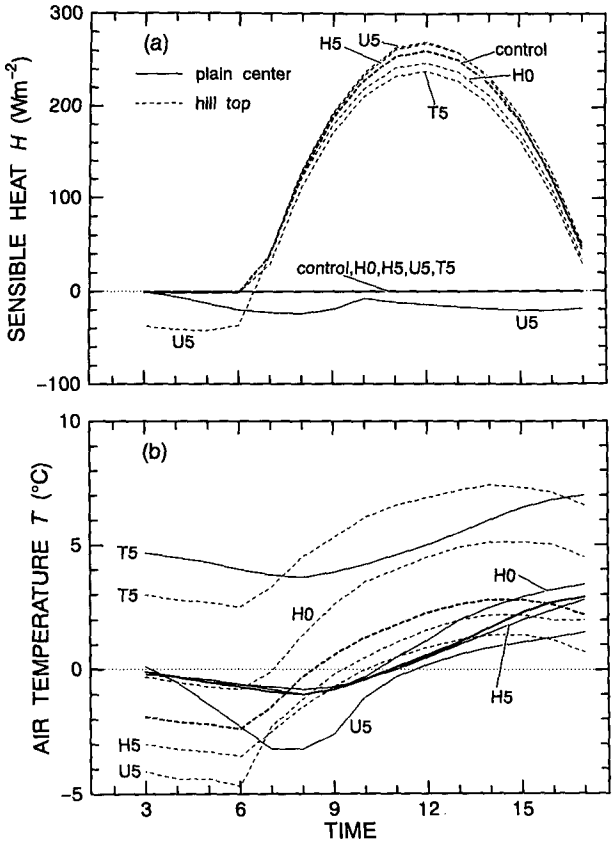

FIG. 10. Time series of (a) sensible heat flux (positive values denote upward flux) and (b) air temperature at the height of 5 m. The solid lines denote the value at the center of the plain and broken lines at the top of the hill. The thick lines denote the control run. The other thin lines denote the results when some parameters are changed; U5: geostrophic wind is 5 m s^{-1}, H5: h_0 = 500 m, H0: h_0 = 0, and T5: T_{Si} = 5°C.

can be assumed that the upper potential temperature and the height of the mixed layer at Sendai and Wajima are close to those at Nagaoka, where no aerological data are available, the maximum air temperature should be close to the potential temperature at 900 hPa. Figure 12 implies that a mixed layer is formed by the influence of forested areas.

The stable layer found in the lower atmosphere (under 300 m) over the plain, as shown in Fig. 9, does not appear when sparse obstacles ($c_* \approx 0.03$) are added to the plain area. In this case ($c_* = 0.03$ over the plain), the upward sensible heat flux is 22 W m^{-2} at maximum and about 10 W m^{-2} on average over the plain. In practice, since a few obstacles such as buildings and trees are found over the plain, the stable layer will not form near the ground. The forest density c_* that was set to 0.3 over the hill is not considered to be realistic. The daytime atmospheric heating exhibits a strong dependence on forest density.

Here, it should be discussed that there are other causes of atmospheric heating during the snowmelt season mentioned in the introduction besides obstacles such as forests. First, the advection is obviously important for the temperature distribution, but it is difficult to estimate quantitatively. As a result, for this paper, it can only be stated that the temperature rise can be explained without advection. Second, direct atmospheric heating by solar radiation should be comparatively large since the albedo of snow surfaces is high. Halberstam and Schieldge (1981) pointed out that a highly stable layer with a raised maximum of temperature formed owing to the radiative absorption during the day. However, it is difficult to regard direct solar heating as the cause of the thick mixed layer. Third, the subsidence of warm air due to terrain features is not considerable over a plain without obstacles such as a forest. Although heat is supplied by the subsidence of warm air according to the two-dimensional calculation, it results from a thermal imbalance. Finally, synoptic-scale subsidence is of the order of 0.01 m s^{-1}; thus, it is less than the subsidence due to the thermal circulation, being of the order of 0.1 m s^{-1}.

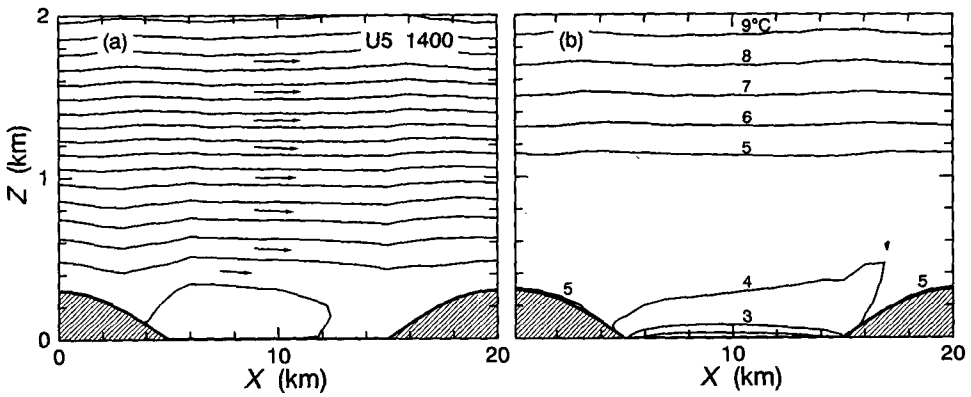

FIG. 11. The same as Fig. 9 except that the geostrophic wind is 5 m s^{-1} (U5). The contour interval of the streamlines is 500 m^2 s^{-1}.

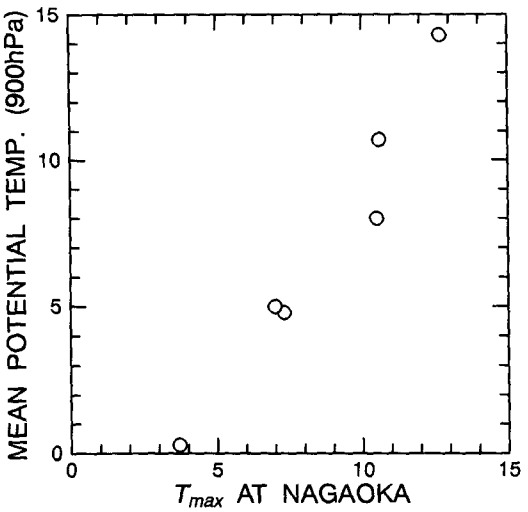

FIG. 12. The relationship between the maximum air temperature observed at Nagaoka and the mean potential temperature at 900 hPa.

5. Concluding remarks

It was shown in data from Niigata Prefecture, a high snowfall area in Japan, that the air temperature could rise above 0°C during the daytime, even when significant snow remained. This temperature rise is marked when the duration of sunshine is long and is not clearly related to wind speed. It was found that the air temperature rose owing to the solar radiation and could rise even further if advection was weak.

Using an atmospheric model combined with heat balance models of forest and snow cover, it was found that a sensible heat flux over forested areas supplied heat to the atmosphere, increasing the temperature to above 0°C. Moreover, it was found that the atmosphere was heated by the subsidence of warm air over an unforested plain if there were forests around the plain.

As a result, it is concluded that one of the main causes of the atmospheric temperature rise during the snowmelt season is the heat flux emitted over forested areas around a plain. Since this type of atmospheric heating occurs everywhere when only forests and snow exist, it is not proper to think that the ground always cools the atmosphere until the snow vanishes. It would be of interest to examine how this mechanism of atmospheric heating works over vast forested areas, such as Siberia and North America, and how it is related to the global climate.

Acknowledgments. The author wishes to thank Professor J. Kondo of Tohoku University for numerous helpful suggestions, and Professor F. Kimura of the University of Tsukuba for his cooperation in the operation of the atmospheric model and for valuable comments.

REFERENCES

Bougeault, P., 1983: A non-reflective upper boundary condition for limited-height hydrostatic models. *Mon. Wea. Rev.*, **111**, 420–429.

Dyer, A. J., and B. B. Hicks, 1970: Flux-gradient relationships in the constant flux layer. *Quart. J. Roy. Meteor. Soc.*, **96**, 715–721.

Halberstam, I., and J. P. Schieldge, 1981: Anomalous behavior of the atmospheric surface layer over a melting snowpack. *J. Appl. Meteor.*, **20**, 255–265.

Kimura, F., and P. Manins, 1988: Blocking in periodic valleys. *Bound.-Layer Meteor.*, **44**, 137–169.

Klemp, J., and D. R. Durran, 1983: An upper boundary condition permitting internal gravity wave radiation in numerical mesoscale models. *Mon. Wea. Rev.*, **111**, 430–444.

Kondo, J., and T. Yamazaki, 1990: A prediction model for snowmelt, snow surface temperature, and freezing depth using a heat balance method. *J. Appl. Meteor.*, **29**, 375–384.

——, and D. Matsushima, 1993: A simple parameterization of longwave radiative cooling with application to the atmospheric boundary layer for clear sky conditions. *Bound.-Layer Meteor.*, **64**, 209–229.

——, O. Kanechika, and N. Yasuda, 1978: Heat and momentum transfers under strong stability in the atmospheric surface layer. *J. Atmos. Sci.*, **35**, 1012–1021.

——, T. Kuwagata, and S. Haginoya, 1989: Heat budget analysis of nocturnal cooling and daytime heating in a basin. *J. Atmos. Sci.*, **46**, 2917–2933.

Segal, M., J. R. Garratt, R. A. Pielke, and Z. Ye, 1991: Scaling and numerical model evaluation of snow-cover effects on the generation and modification of daytime mesoscale circulations. *J. Atmos. Sci.*, **48**, 1024–1042.

Whiteman, C. D., 1982: Breakup of temperature inversions in deep mountain valleys. Part I. Observations. *J. Appl. Meteor.*, **21**, 270–289.

——, 1990: Observations of thermally developed wind systems in mountainous terrain. *Atmospheric Processes over Complex Terrain, Meteor. Monogr.*, No. 45, Amer. Meteor. Soc., 5–42.

Yamazaki, T., and J. Kondo, 1992: The snowmelt and heat balance in snow-covered forested areas. *J. Appl. Meteor.*, **31**, 1322–1327.

——, and ——, 1993: The atmospheric heating over snow-covered forested areas and snowmelt. *Exchange Processes at the Land Surface for a Range of Space and Time Scales, Proc. IAMAP-IAHS Symp.*, Yokohama, Japan, 447–452.

——, ——, T. Watanabe, and T. Sato, 1992: A heat-balance model with a canopy of one or two layers and its application to field experiments. *J. Appl. Meteor.*, **31**, 86–103.